



## Institut für Numerische Simulation

Rheinische Friedrich-Wilhelms-Universität Bonn

Wegelerstraße 6 • 53115 Bonn • Germany  
phone +49 228 73-3427 • fax +49 228 73-7527  
[www.ins.uni-bonn.de](http://www.ins.uni-bonn.de)

Jorge S. Dolado, Michael Griebel, Jan Hamaekers and  
Frederik Heber

### The nano-branched structure of cementitious calcium-silicate-hydrate gel

INS Preprint No. 1008

December 2010



# The nano-branched structure of cementitious calcium-silicate-hydrate gel

Jorge S. Dolado,<sup>a,b</sup> Michael Griebel,<sup>c,d</sup> Jan Hamaekers<sup>c,d</sup> and Frederik Heber<sup>c</sup>

Manipulation of concrete at the nanoscale is severely limited by the lack of precise knowledge on the nanostructure of Calcium Silicate Hydrate gel, the main binding phase of cement-based materials. Here we report a computational description of C-S-H, which by the first time reconciles the existing structural and colloidal/gel-like models. Our molecular dynamic simulations predict the formation of a branched three dimensional C-S-H solid network where the segmental branches (SB) are  $\sim 3 \times 3 \times 6$  nm-sized. The presented simulations account well for the features observed through Small Angle Neutron Scattering (SANS) experiments as well with various observations made by synchrotron X-ray, Nuclear Magnetic Resonance (NMR), and Inelastic Neutron Spectroscopy (INS) measurements and lead to a better understanding of the cementitious nanostructure formation and morphology.

## Introduction

Calcium–silicate–hydrate (C–S–H)<sup>1</sup> gel is the most important hydration product of cement-based materials. It constitutes about 60–70% of the fully hydrated cement paste and is responsible for most of the engineering properties<sup>1</sup> of cement-based materials. The nature of C–S–H gel is certainly complex and still under debate. In fact, the current description of C–S–H gel combines two complementary visions, each one explaining different phenomena on different scales.

At the molecular level, it is well known that C–S–H gel consists of silicate chains held together by calcium oxide layers, as schematically depicted in Fig. 1a. In fact, several structural models have been proposed so far<sup>2–4</sup> that draw structural analogies with two crystalline minerals; tobermorite ( $\text{Ca}_5\text{Si}_6\text{O}_{16}(\text{OH})_2 \cdot 7\text{H}_2\text{O}$ )<sup>5</sup> and jennite ( $\text{Ca}_9\text{Si}_6\text{O}_{18}(\text{OH})_6 \cdot 8\text{H}_2\text{O}$ ).<sup>6</sup> Based on insights gained experimentally, these models represent the C–S–H nanostructure as a mixture of tobermorite and jennite structures in which these layered species show multiple imperfections. Indeed, recent bulk molecular simulations<sup>7</sup> have suggested that C–S–H gel is so defected that it should be considered glassy at very short distances while maintaining certain crystalline ordering at distances of the order of the interlayer spacing.

basic C–S–H particles and described the C–S–H gel as a colloid made of small bricks, where each brick represents gel substance together with its associate gel pores. The current viewpoint is the Jennings' model (JM),<sup>12,13</sup> which can be viewed as a hybrid of the F&S and P&B models. It incorporates the insights gained from the neutron and X-ray scattering measurements,<sup>14,15</sup> which reveal the existence of 4 nm-sized C–S–H features to propose a new model where the C–S–H gel is made up of the aggregation of 4 nm-sized bricks, as sketched in Fig. 1b. This model essentially focuses on the state of water in both the interlayer spaces of the bricks and gel pores to interpret previous sorption.

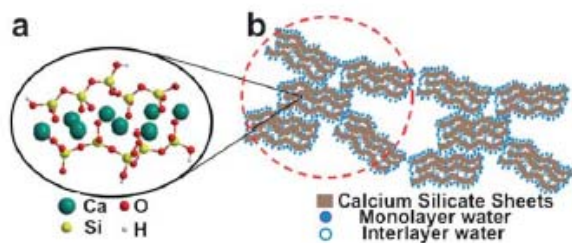


**Fig. 1** A schematic representation of the current description of C–S–H gel. This figure represents schematic representations of the classical microstructural viewpoint (a), which relies on tobermorite and jennite morphologies, and the Jennings model (JM) (b), which is the modern colloidal/gel-like conception of C–S–H gel.

Measurements<sup>10,16</sup> and quantify the density and water content of C–S–H at different relative humidity conditions.

However, and in spite of the knowledge already gained over the past few decades, nagging questions persist regarding the true structure of C–S–H gel. As explained before, neutron scattering experiments<sup>14,15</sup> predict the existence of  $\sim 4$  nm-sized C–S–H features from which the whole C–S–H structure is assembled, but questions considering the how and why of the formation of these structural units remain unanswered. Likewise, the possible linkage between the structural models based on layered tobermorite and jennite pieces and the real composition of these 4 nm-sized C–S–H features remains a challenging question. It seems clear that a new model capable of bringing together the molecular and colloidal/gel-like viewpoints is greatly needed.

The model presented herein is the first one that enables researchers to deal with the molecular/structural and colloidal/gel-like approaches on an equal footing. To this end, we analyze the formation of C–S–H particles by the method of

<sup>a</sup>Tecnalia R&I, Parque Tecnológico de Bizkaia, 48160 Derio, Bizkaia, Spain. E-mail: [jorge.dolado@tecnalia.com](mailto:jorge.dolado@tecnalia.com)

<sup>b</sup>Nanostructured and Eco-efficient Materials for Construction Unit, Associated Unit LABEIN-Tecnalia, CSIC, Spain

<sup>c</sup>Department of Numerical Simulation, University of Bonn, Wegelerstraße 6, D-53115 Bonn, Germany

<sup>d</sup>Fraunhofer Institute for Algorithms and Scientific Computing SCAI, D53754 Sankt Augustin, Germany

At larger scales, existing models of C–S–H have been mainly focused on the recognition of the colloidal and gel-like properties of C–S–H gel. Two differentiated schools of thought exist in the literature. On the one hand, there are the works of Feldman and Sereda (F&S) and others,<sup>8,9</sup> which regard the C–S–H gel as a three-dimensional assemblage of irregular C–S–H layers with adsorbed water and interlayer water molecules. On the other hand, there are the works of Power and Brownyard (P&B) and others<sup>10,11</sup> that have emphasized the existence of

<sup>1</sup> C = CaO, S = SiO<sub>2</sub> and H = H<sub>2</sub>O, commonly used by the cement chemistry community. C–S–H is used as an abbreviation for calcium–silicate–hydrates at an unspecified mass ratio.

molecular dynamics simulations. The employed methodology rests on the study of the formation of C–S–H structures resulting from the polymerization of  $\text{Si(OH)}_4$  in the presence of solvated calcium ions ( $\text{Ca(OH)}_2 \cdot 4\text{H}_2\text{O}$ ). It is worth noting that contrary to most atomistic attempts, which assume crystalline tobermorite- or jennitelike structures,<sup>7,17,18</sup> our computational scheme reproduces the formation of C–S–H structures without imposing any structural model. A previous work of the authors<sup>19</sup> proved that this approach naturally gives useful chemical information, such as the number of Si–O–Si, Si–OH and Ca–OH bonds, in terms of the Ca/Si ratio of the C–S–H particles. In this work, new algorithms have been developed and implemented to monitor the process of formation of C–S–H clusters and to account for important physical features of the C–S–H particles. As is usual in most studies,<sup>1,15</sup> we limit our description to a C–S–H gel with Ca/Si = 1.7.

## Computational methods

### Molecular dynamic simulations

We have used the same force field formalism as employed in a previous work of the authors;<sup>19</sup> namely a scheme of Feuston and Garofalini.<sup>20</sup> Here, the overall potential energy function is composed of a modified Born–Mayer–Huggins (BMH) two-body interaction term and a three-body interaction term similar to the well-known Stillinger–Weber<sup>21</sup> potential. To account for the Si, O and H interactions we adopted the improved variant of Litton and Garofalini, which accounts especially well for the polymerization of silica sols ( $\text{Si(OH)}_4$  monomers) and condensation reactions. The detailed potential functions and parameters can be found in the literature.<sup>22</sup> Let us observe that the growth of the C–S–H structure can be viewed as a sol-gel process in which silica sols ( $\text{Si(OH)}_4$ ) polymerise in a calcium rich environment. To incorporate the effect of Ca ions into the silica sol polymerisation we model the Si, O and Ca interactions through the parametrization given by Su and Garofalini.<sup>23</sup> Additionally, we apply a screened Coulomb potential term  $q_i^* q_j^* / r_{ij} \text{erfc}(r_{ij}/\beta_{ij})$  to represent the repulsive interaction of Ca and H. Here,  $q_i$  denotes the ionic charge of particle i,  $r_{ij}$  denotes the distance between particle i and particle j,  $\beta_{ij}$  is an interaction-dependent parameter, and erfc stands for the complementary error function. For the parameter  $\beta_{ij}$  we use a value of 2.31 Å for an atom pair Ca–H. The ionic charges for calcium ions and hydrogen are +2 and +1, respectively.

Molecular dynamics simulations have been executed with TREMOLO-X,<sup>24</sup> a load-balanced, memory-distributed, parallel code, written at the Institute for Numerical Simulation. The simulations were performed in a canonical ensemble with constant particle number ( $N$ ), constant volume ( $V$ ) and constant temperature ( $T$ ) and periodic boundary conditions. For further details on the time evolution formalism and the predictor–corrector time-integrator we refer the reader to ref. 19.

To ensure that several 4 nm C–S–H features could be observed in the simulations, 1511  $\text{Si(OH)}_4$  and 2585  $\text{Ca(OH)}_2 \cdot 4\text{H}_2\text{O}$  molecules (roughly 60 000 atoms) have been simulated in a square box with dimensions 8.8 nm for a total duration of 2.3 ns with a time step of ~0.1 fs. Snapshots of the atomic positions have been generated every 10 ps. They consist of the C–S–H cluster and water molecules.

### Identification of the C–S–H clusters and the SBs

In order to separate the C–S–H cluster from the water molecules of the solution, a modified Connected Components Analysis algorithm<sup>25</sup> has been used on the results of the molecular dynamics simulation. Inertia tensors are used to identify connected components or clusters. Once the covalently linked structure has been determined, the amount of water that is chemically tied to the surface of the solid cluster is assessed by energy considerations. According to our analysis, the transition from chemical to physical binding occurs at  $\tau = 3$  Å, where the adsorption energy of one molecule of water is lower than 1 eV. After the C–S–H cluster has been isolated, we have executed a Delaunay triangulation of the surface of the cluster with an algorithm similar in spirit to the ‘rolling sphere’ algorithm of Shrake and Rupley<sup>26</sup> with varying probe radii. By comparing different resulting triangulations, the local concavity has been measured. Via a simplified Approximate Convex Decomposition approach,<sup>27</sup> the cluster is then separated into approximately convex pieces. After all of these convex pieces have been assembled, their principal axis system resulting from the inertia tensor then gives a classification of the general ellipsoidal shape. In this way we obtain the physical features of the Segmental Branches (SB).

### SANS and X-ray patterns

The theoretical simulations of the SANS and X-ray spectra have been calculated according to the Debye equation as implemented in the Debyer package.<sup>28</sup> In the case of the X-ray analysis the wavelength of the Cu K $\alpha$  radiation (0.154 nm) has been employed for the comparisons.

## Results and discussion

### The nano-branched structure of C–S–H gel

In Fig. 2a we show the last snapshot of our simulations, in which a three-dimensional C–S–H structure can be recognized. This structure comprises a solid body formed by covalently linked atoms together with chemically adsorbed water molecules. Let us also note that the result seen in Fig. 2a is actually a branched network, as the 2 × 2 × 2 supercell reconstruction shown in Fig. 2b makes evident. We rationalize this C–S–H structure as resulting from the interweaving and restructuring process of growing C–S–H segments. Let us note that the branched structure resulting from our simulations is similar to that already proposed by the F&S model,<sup>8</sup> in the sense that no separate C–S–H bricks can be identified at the scale under study, although certain analogies can also be established with JM (see the structures enclosed by red circles in Fig. 1 and Fig. 2). As explained in the Methods section, for each snapshot a cluster identification protocol and a surface recognition procedure have allowed us to identify Segmental Branches (SB) as regions of the cluster where the surface concavity is minimal. The C–S–H cluster of the last snapshot is shown in Fig. 2c. One example of SB is indicated in Fig. 2c and by a close-up of the dashed box (Fig. 2d). According to our analysis, the SBs correspond to ~3 × 3 × 6 nm-sized C–S–H pieces.

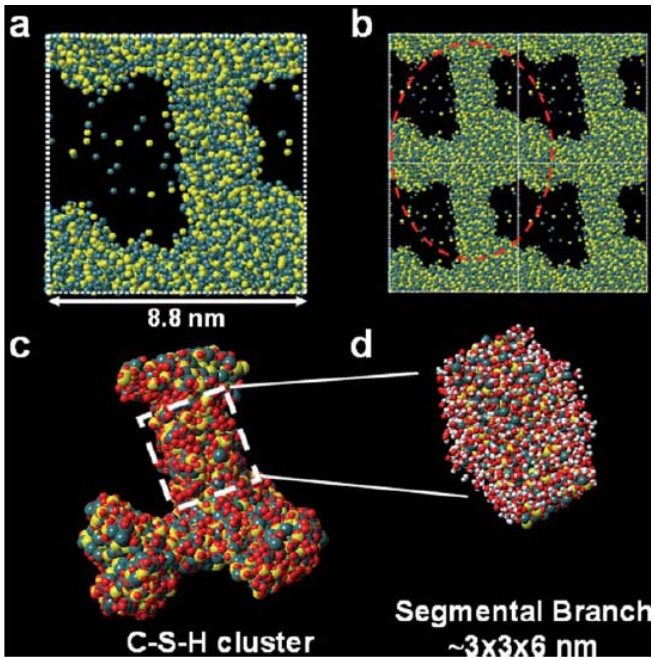


**Fig. 2** (a) The last snapshot of our simulation, where the hydrogen atoms are not shown for clarity. (b) The  $2 \times 2 \times 2$  supercell reconstruction of the last snapshot. (c) The three-dimensional cluster appearing after the employed cluster recognition analysis. The chemically adsorbed water molecules are hidden for clarity. (d) The atomic structure of the Segmental Branches (SB). Employed notation: green = Ca atoms, yellow = Si atoms, red = O atoms and white = H atoms.

#### Comparison with SANS measurements

To further assess the soundness of the computed branched structure of Fig. 2c, we calculated its theoretical neutron scattering intensity based on the Debye equation<sup>29</sup> as implemented in the Debye package.<sup>28</sup> In Fig. 3a, we compare our predicted intensity (circles) with the experimental data obtained by SANS measurements<sup>14</sup> (line) as a function of the magnitude of the scattering vector  $Q$ . As can be seen, the computed scattering intensity matches perfectly the SANS intensity data for  $Q$  vectors higher than  $Q \geq 0.5 \text{ nm}^{-1}$ . Note also that our theoretical neutron scattering intensity is able to reproduce the cross-over behavior found for the slope of the intensity, jumping from a volume fractal regime (described by a power law  $Q^{-D_v}$  dependence, with  $2 < D_v < 3$ ) to the so-called Porod scattering regime ( $Q^{-4}$  law). This last regime is governed by the scattering of the smallest features, i.e. the SBs according to our simulations. Though the SBs cannot be considered as independent C-S-H particles, it is worth noting that their dimensions ( $\sim 3 \times 3 \times 6 \text{ nm}$ ) match well with those of the features observed by the SANS measurements ( $\sim 4 \text{ nm}$ ). To investigate this point in greater detail, we calculated the Form Factor of a  $3 \times 3 \times 6 \text{ nm}$  ellipsoid as a function of the magnitude of the scattering vector  $Q$ . The SANS intensity resulting from the Form Factor is displayed in Fig. 3a with a green dashed line. As can be seen, the Form Factor of  $3 \times 3 \times 6 \text{ nm}$ -sized ellipsoids suffices to reproduce the experimental data within the Porod regime. This novel result unambiguously confirms that the shape and size found in our simulations for the SBs are meaningful.

#### Comparison with NMR, INS and XRD

Following the formalism detailed in ref. 19, we analyzed the connectivity of the silicate chains of C-S-H and the number of Ca–OH and Si–OH bonds. As presented in the ESI†, our numerical experiments predict values fairly consistent with the inferences gained from NMR<sup>2</sup> and by INS experiments<sup>30</sup> and they allow us to conclude that Fig. 2c actually contains certain short range features consistent with concurrent tobermorite- and jennite-like environments. In Fig. 3b we compare the simulated X-ray pattern of the SBs (blue line) with the patterns measured in ref. 31 (red line) and in ref. 32 (green line) for synthetic C–S–H samples. While this last experimental pattern has sharp peaks (black dots), the synchrotron measurements<sup>31</sup> and our simulated diffractogram yield wider peaks.

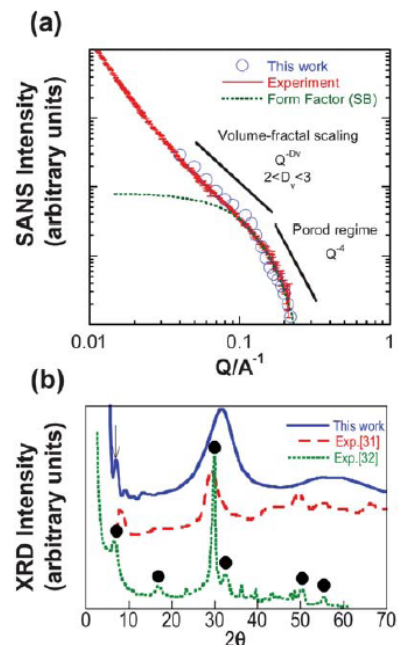


**Fig. 3** Characterization of our simulated clusters. (a) Comparison between the theoretical SANS spectra with the experimental values obtained in ref. 14. (b) Comparison between our theoretical X-ray pattern and the experimental ones.<sup>31,32</sup> The important reflections (solid points) are also indicated by their associated diffraction distances (nm).

In fact, the broadening of the peaks (together with a novel application of pair distribution functions techniques) was employed in ref. 31 to reveal that C–S–H has no correlated structure past  $\sim 3.5 \text{ nm}$  and to propose the existence of nano crystalline C–S–H particles of  $3.5 \text{ nm}$  in diameter. Let us note that these sizes agree well with the sizes of our SBs. On the other hand, our computed C–S–H varieties present quite an amorphous X-ray character, with two broad reflections centered at  $55^\circ$  and  $31^\circ$  and a well-defined peak at  $7^\circ$ . This last peak corresponds to a  $d$  spacing of  $\sim 1.2 \text{ nm}$  and can be recognized as the typical basal reflection present in all tobermorite- and jennite-like arrangements. Essentially our simulated C–S–H structure, like the one proposed in ref. 7 can be considered glassy for short range distances while maintaining some layered features at longer distances

associated with the interlayer spacing. Nevertheless, it is worth noting that in spite of the reasonable agreement with the measurements, the experimental XRD patterns clearly show more structural detail (*e.g.* peaks at 50° and 60°) than the one inferred from the simulations. This discrepancy can partially be attributed to the lower Ca/Si ratio of the experimental C–S–H samples (something that is known to favor the crystallinity), but the intrinsic limits of the MD techniques cannot be ruled-out either. Obviously, further in-depth work is needed in this direction.

### C–S–H SBs' composition and densities

From our simulations it is straightforward to estimate the densities of the SBs at different humidity conditions by varying the water film thickness  $\tau$ . In Fig. 4a we present our densities (solid points) as a function of the water content (expressed in mol of H per mol of C–S–H) and as function of the thickness ( $\tau$ ). For comparison we also show the estimations of JM (circles). As can be seen, our numerical predictions agree fairly well with the estimations of JM and allow us to distinguish some important C–S–H states in terms of their water content. The dried C–S–H skeleton corresponds to  $\tau = 0 \text{ \AA}$ ;  $\text{C}_{1.7}\text{SH}_{0.85}$ ;  $2.85 \text{ g cm}^{-3}$ . The *d*-dried C–S–H state (*i.e.* one containing only non-evaporable water<sup>13</sup>) corresponds to  $\tau = 1.5 \text{ \AA}$ ,  $\text{C}_{1.7}\text{SH}_{1.2}$ ;  $2.65 \text{ g cm}^{-3}$ . The saturated solid C–S–H particle addressed in JM can be identified in our simulations as a state with  $\tau = 2.5 \text{ \AA}$ ;  $\text{C}_{1.7}\text{SH}_{1.65}$ ;  $2.58 \text{ g cm}^{-3}$ . Finally, when a complete monolayer of water is adsorbed, our C–S–H state corresponds to  $\tau = 3 \text{ \AA}$ ;  $\text{C}_{1.7}\text{SH}_{2.2}$ ;  $2.42 \text{ g cm}^{-3}$ . Thomas *et al.*<sup>33</sup> have recently discussed the higher

containing “intrinsic” water content only, also illustrates the significantly different behavior of water near the surface from its bulk state.

### Comparison with sorption/desorption measurements

We finally compared the thicknesses of our water layers with those determined empirically by water adsorption/desorption measurements using the so called *t*-curve.<sup>34</sup> To this end, we changed from our water content predictions to relative humidity (RH (%)) with the aid of JM. In Fig. 4b our results (points) are compared with the experimental measurements of Badmann *et al.*<sup>35</sup> (inverse triangles) and those of Hagymassy *et al.* (triangles).<sup>36</sup> Given the experimental difficulties in obtaining accurate estimations at very low relative pressures and given the possible errors occurring from the small mismatch between the water content of the *d*-dried C–S–H state in the JM (H = 1.3) and our case (H = 1.2), it is clear that our results show a more than reasonable agreement with the experiments.

## Conclusions

In summary, a new model of C–S–H gel has been presented, which reconciles, in a single picture, the microstructural and colloidal/gel-like viewpoints. In essence, our atomistic simulations predict the appearance of a branched three-dimensional C–S–H nanostructure, which provides for the first time a satisfactory comparison with the SANS and water sorption/desorption measurements, while concurrently accounting reasonably well for the microstructural information gained from NMR, XRD and INS experiments. Besides, the origin of such a branched structure is explained as resulting from a restructuring process of growing C–S–H segments. It is also noteworthy that our simulations recognized  $3 \times 3 \times 6 \text{ nm}$ -sized SBs, something that matches well with the existence of  $3.5\text{--}4.0 \text{ nm}$  C–S–H features, as proposed by synchrotron XRD and SANS measurements. Nevertheless, it should be recognized that our study was limited to C–S–H gels with  $\text{Ca/Si} = 1.7$ ; *i.e.* the mean value found in ordinary portland cements. As the precise morphology of the SBs might depend on the Ca/Si ratio, further research in this direction is currently underway. In any case, it seems clear that our results lead to an unprecedented understanding of the cementitious nanostructure formation and are a strong basis to improve the mechanical and durability properties of cement-based materials.

## Acknowledgements

The financial support of the FP7 program of the European Commission (CODICE project; contract NMP3-SL-2008-214030) is gratefully acknowledged. The computing resources of CESGA are also acknowledged. Finally J.S.D thanks A. Ayuela, H. Manzano, S. Arrese-Igor and S. Cerveny for fruitful suggestions and comments.

## Notes and references

- 1 M. Vandamme and F.-J. Ulm, Proc. Natl. Acad. Sci. U. S. A., 2009, **106**, 10552.
- 2 X. Cong and R. J. Kirkpatrick, Adv. Cem. Based Mater., 1996, **3**, 144.

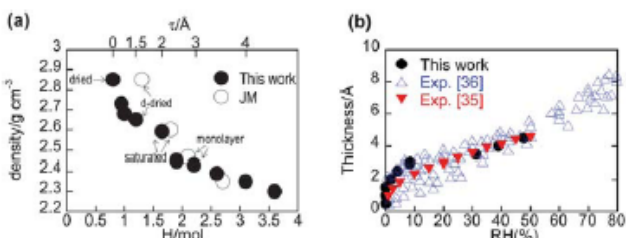


**Fig. 4** C–S–H gel at different relative humidity conditions. (a) Computed densities as a function of the water content ( $H$ ) and as a function of the thicknesses ( $\tau$ ). The results are compared with the estimations of JM.<sup>16</sup> (b) Computed *t*-curve compared with the empirical results of Badmann *et al.*<sup>35</sup> and Hagymassy *et al.*<sup>36</sup>

density of C–S–H compared to that of tobermorite and jennite, suggesting a plausible explanation based on both a highly defective C–S–H solid structure and on surface effects related to its nano-particulate morphology. It is remarkable that our results corroborate this hypothesis. Though a detailed discussion on the different states of water in C–S–H will be presented elsewhere, our simulations recognize two distinguishable types of adsorbed water molecules. While at low coverage ( $\tau < 2.5 \text{ \AA}$ ) the water molecules are essentially tied to the surface by strong hydrogen bonds with the hanging Ca-OH and Si-OH bonds, at larger coverage ( $\tau > 2.5 \text{ \AA}$ ) the water molecules mainly participate in the structure by water–water hydrogen bonds. This finding, which can explain why the solid-saturated state ( $\tau = 2.5 \text{ \AA}$ ) can be seen as the state

- 3 H. F. Taylor, *J. Am. Ceram. Soc.*, 1986, **69**, 464.  
 4 I. G. Richardson and G. W. Groves, *Cem. Concr. Res.*, 1992, **22**, 1001.  
 5 E. Bonaccorsi, S. Merlini and A. R. Kampf, *J. Am. Ceram. Soc.*, 2005, **88**, 505.  
 6 E. Bonaccorsi, S. Merlini and H. F. W. Taylor, *Cem. Concr. Res.*, 2004, **34**, 1481.  
 7 R. J.-M. Pellenq, *et al.*, *Proc. Natl. Acad. Sci. U. S. A.*, 2009, **106**, 16102.  
 8 R. F. Feldman and P. Sereda, *J. Eng. J. Can.*, 1970, **53**, 53.  
 9 M. Daimon, S. A. Abo-Enein, G. Hosaka, S. Goto and R. Kondo, *J. Am. Ceram. Soc.*, 1977, **60**, 110.  
 10 T. C. Powers, T. L. Brownlyard, *Studies of the Physical Properties of Hardened Portland Cement Paste (Selected Landmark papers in Concrete Materials Research)*, SP-249 American Concrete Institute, Michigan, 2008.  
 11 S. Brunauer, *American Scientist*, 1962, **50**, 210.  
 12 H. M. Jennings, *Cem. Concr. Res.*, 2000, **30**, 101.  
 13 H. M. Jennings, *Cem. Concr. Res.*, 2008, **38**, 275.  
 14 A. J. Allen, J. J. Thomas and H. M. Jennings, *Nat. Mater.*, 2007, **6**, 311.  
 15 A. J. Allen, R. C. Oberthur, D. Pearson, P. Schofield and C. R. Wilding, *Phil. Mag. B*, 1987, **56**, 263.  
 16 R. F. Feldman, *Cem. Concr. Res.*, 1972, **2**, 489–492.  
 17 A. G. Kalinichev, J. Wang and R. J. Kirkpatrick, *Cem. Concr. Res.*, 2007, **37**, 337–347.  
 18 H. Manzano, J. S. Dolado and A. Ayuela, *Acta Mater.*, 2009, **57**, 1666.  
 19 J. S. Dolado, M. Griebel and J. Hamaekers, *J. Am. Cer. Soc.*, 2007, **90**, 3938.  
 20 B. P. Feuston and S. H. Garofallini, *Chem. Phys. Lett.*, 1990, **170**, 264.  
 21 F. Stillinger and T. Weber, *Phys. Rev. B*, 1985, **31**, 5262.  
 22 D. A. Litton and S. H. Garofalini, *J. Appl. Phys.*, 2001, **89**(11), 6013.  
 23 X. Su and S. H. Garofalini, *J. Mater. Res.*, 2004, **19**, 3679.  
 24 M. Griebel, S. Knapek, G. Zumbusch, *Numerical Simulation in Molecular Dynamics*, Springer, Berlin, 2007.  
 25 J. Hopcroft and R. Tarjan, *Commun. ACM*, 1973, **16**, 372.  
 26 A. Shrake and J. A. Rupley, *J. Mol. Biol.*, 1973, **79**, 351.  
 27 J. Lien and N. Amato, *Comp. Geom.*, 2006, **35**, 100.  
 28 <http://www.unipress.waw.pl/debyer/>.  
 29 P. Debye, *Ann. Phys.*, 1915, **46**, 809.  
 30 J. J. Thomas, J. Chen, H. M. Jennings and D. A. Neumann, *Chem. Mater.*, 2003, **15**, 3813.  
 31 L. B. Skinner, S. R. Chae, C. J. Benmore, H. R. Wenk and P. J. M. Monteiro, *Phys. Rev. Lett.*, 2010, **104**, 195502.  
 32 S. Suzuki and E. Sinn, *J. Mater. Sci. Lett.*, 1993, **12**, 542.  
 33 J. J. Thomas, H.M. Jennings and A. J. Allen, *J. Phys. Chem. C*, 2010, **114**, 7594.  
 34 K. K. Aligizaki, *Pore structure of cement-based materials*, Taylor & Francis, Oxon, 2006.  
 35 R. Badmann, N. Stockhausen and M. J. J. Setzera, *J. Colloid Interface Sci.*, 1981, **82**(2), 534.  
 36 J. Hagymassy, S. Brunauer and R. Mikhail, *J. Colloid Interface Sci.*, 1969, **29**(3), 485.